EARTHQUAKE SPECTRA

The Professional Journal of the Earthquake Engineering Research Institute

PREPRINT

This preprint is a PDF of a manuscript that has been accepted for publication in *Earthquake Spectra*. It is the final version that was uploaded and approved by the author(s). While the paper has been through the usual rigorous peer review process for the Journal, it has not been copyedited, nor have the figures and tables been modified for final publication. Please also note that the paper may refer to online Appendices that are not yet available.

We have posted this preliminary version of the manuscript online in the interest of making the scientific findings available for distribution and citation as quickly as possible following acceptance. However, readers should be aware that the final, published version will look different from this version and may also have some differences in content.

The DOI for this manuscript and the correct format for citing the paper are given at the top of the online (html) abstract.

Once the final, published version of this paper is posted online, it will replace the preliminary version at the specified DOI.

Non-linear dynamic analysis of a full-scale unreinforced adobe model

Nicola Tarque Ruíz,[a)b)c)] Guido Camata,[c)] Enrico Spacone,[c)] Humberto Varum[d)] M.EERI, and Marcial Blondet[a)] M.EERI

This paper describes the results of a numerical study of a full-scale adobe building model tested on a shaking table. Material properties of adobe masonry were calibrated to represent the wall in-plane seismic behaviour, based on a previous numerical analysis of an adobe wall carried out by the authors. The inelastic part of the constitutive model was represented by a softening curve in tension and by a hardening/softening behaviour in compression, thus the fracture energy is a key issue in the modelling process. A finite element model that relies on a homogenous continuum approach was developed in Abaqus/Explicit software. The damage evolution in the numerical simulation represented fairly well the experimental crack pattern, for in-plane and out-of-plane seismic effects. Overall, the calibrated material properties and the explicit solution scheme proved to be appropriate for simulating the seismic behaviour and predicting capacity of unreinforced adobe structures subjected to seismic loading.

INTRODUCTION

Adobe is a Spanish word derived from the Arabic *atob*, which literally means sun-dried brick. It is one of the oldest and most widely used natural building materials, especially in Latin America, the Middle East and north and south Africa. For example, earth constructions constitute around 43% of the total building stock in Peru (INEI 2008). Figure 1 shows some typical Peruvian adobe dwellings located in the countryside along the coast and in the highlands.

[a)] Division of Civil Engineering, Pontificia Universidad Católica del Perú, Av. Universitaria 1801, Lima 32, Peru.
[b)] ROSE School, IUSS Pavia, Via Ferrata 1, 27100 Pavia, Italy.
[c)] Department of Engineering, Università degli Studi 'G. D'Annunzio' Chieti-Pescara. Viale Pindaro 42, 65127 Pescara, Italy.
[d)] Department of Civil Engineering, University of Aveiro. 3810-193, Aveiro, Portugal.

(a)  (b) 

Figure 1. Typical Peruvian adobe houses, (a) adobe house located in the Peruvian coast, (b) adobe house located in the Peruvian highlands.

Adobe constructions have some attractive characteristics, such as low cost, use of locally available materials, good thermal insulation and acoustic properties (Memari and Kauffman 2005). This is usually non-engineered construction, since there is no need for skilled labour, and in several countries adobe dwelling are built by owners themselves. However, adobe structures are quite vulnerable to seismic effects, largely due to weak mechanical properties of adobe blocks, poor construction techniques, and their heavy weight (Tarque *et al.* 2012). Adobe structures are widely used for single-family housing in lesser developed countries, research evidence related to the seismic response of adobe buildings is limited, hence there is a strong need for experimental and analytical studies to investigate seismic behaviour of adobe buildings, improve their dynamic performance, and reduce their seismic vulnerability.

One of the biggest challenges related to modelling adobe constructions is the characterization of their material properties, particularly in the inelastic range. Unlike other materials, there is a limited experimental test data related to mechanical properties of adobe units and mud mortar (e.g. compression tests on adobe piles, diagonal compression tests on adobe wallets and shear tests on adobe walls). The available experimental data provides information on mechanical properties in elastic range (Blondet and Vargas 1978), however due to extremely brittle soil behaviour it is difficult to obtain reliable experimental data for the inelastic range. In order to define the inelastic parameters necessary to model the adobe material properties for non-linear analyses, Tarque (2011) gathered information from the previous experimental studies on adobe material properties. Unknown parameters were numerically calibrated to simulate the experimental cyclic behaviour of adobe walls. Information regarding these material properties is given in Table 1 and

Table 2.

This paper presents the results of dynamic analyses of an adobe building model tested in 2005 (Blondet *et al.* 2006) on the shaking table at the Pontificia Universidad Católica del Perú. The building was modelled using a non-linear finite element model in Abaqus/Explicit software. The continuum damage plasticity model was used to simulate the behavior of adobe masonry.

FINITE ELEMENT MODEL

Behaviour of masonry materials can be modelled following a discrete or a continuum mechanics approach (*e.g.* Lotfi and Shing 1994; Lourenço 1996; Ngo and Scordelis 1967; Page 1978; Pelà 2008; Roca *et al.* 2010; Rots 1991). The first approach assumes that damage is concentrated at specific zones to simulate the block-to-block and block-to-mortar interaction (Roca *et al.* 2010). Generally, the inelastic behaviour is concentrated at the mortar joints where tensile, shear and compressive failure can take place. This model assumes elastic behavior of adobe bricks. The discrete model accurately represents the behaviour of masonry structures when the failure mechanism and the crack path follow the mortar joints. The second approach uses the continuum model which assumes cracking and damage to be distributed within the homogeneous continuum masonry medium. Interaction between bricks and mortar is not explicitly considered in the model. In both models, the crack propagation is mainly controlled by the shape of the softening diagram and the material tensile fracture energy since masonry has low tensile strength (Cruz *et al.* 2004). Figure 2 shows an example of a 1.93 m high adobe wall subjected to horizontal displacement applied atop the wall, which is modelled both by a discrete and a continuum model. In the case of discrete model, the mud mortar is modelled with interface elements which allow the physical separation of adobe blocks. Concrete beams were provided at the base and the top of the wall.

The failure assessment of brittle materials such as concrete and masonry mainly depends on the material constitutive laws used (Feenstra and de Borst 1992; Feenstra and Rots 2001). Similarly to concrete, adobe masonry behaves well under compression, but its ability to resist tensile stresses is limited and characterized by a brittle post-peak tensile response. Since adobe bricks and mortar are composed of mud, an adobe wall can be reasonably assumed to be homogeneous and isotropic.

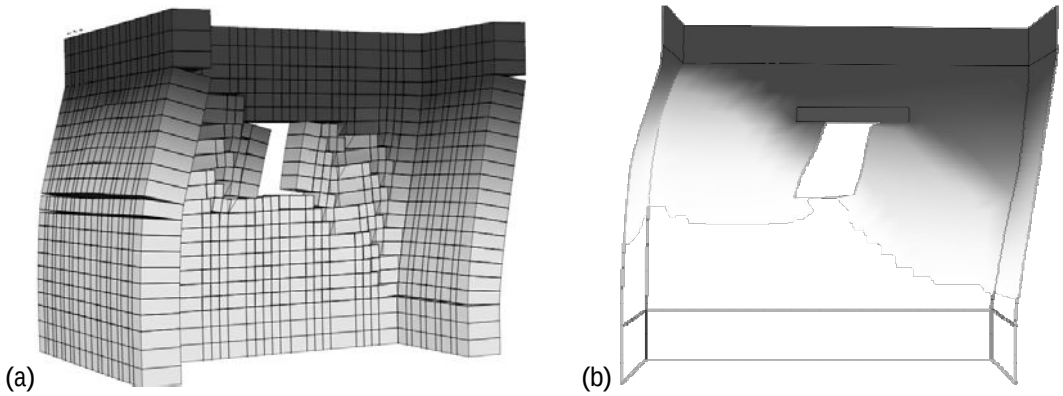

Figure 2. Deformation patterns of the numerical models developed by Tarque 2011 for simulating the in-plane response of an adobe wall under a monotonically applied wall top displacement using (a) discrete and (b) continuum approaches.

The adobe model examined in this paper is composed of adobe bricks, mud mortar, concrete foundations and a timber roof. The adobe bricks and the mud mortar are considered homogenous and modelled with the concrete damage plasticity model (continuum approach) implemented in Abaqus/Explicit (Abaqus 6.9 SIMULIA 2009).

The damage plasticity model is based on the classical plasticity theory and it is applicable to quasi-brittle materials subjected to cyclic loads such as concrete. It uses concepts of isotropic damage elasticity in combination with isotropic tensile and compressive plasticity to simulate the inelastic behaviour of a material. The concrete damage plasticity model is based on the work by Lubliner *et al.* (1989) and Lee and Fenves (1998), and the two main failure mechanisms are tensile cracking and compressive crushing. This model decomposes the total strain into the elastic and plastic strain ($\varepsilon = \varepsilon_e + \varepsilon_p$) and it assumes that material failure can be effectively modelled using its uniaxial tensile, uniaxial compressive, and plasticity characteristics (Figures 3 and 4).

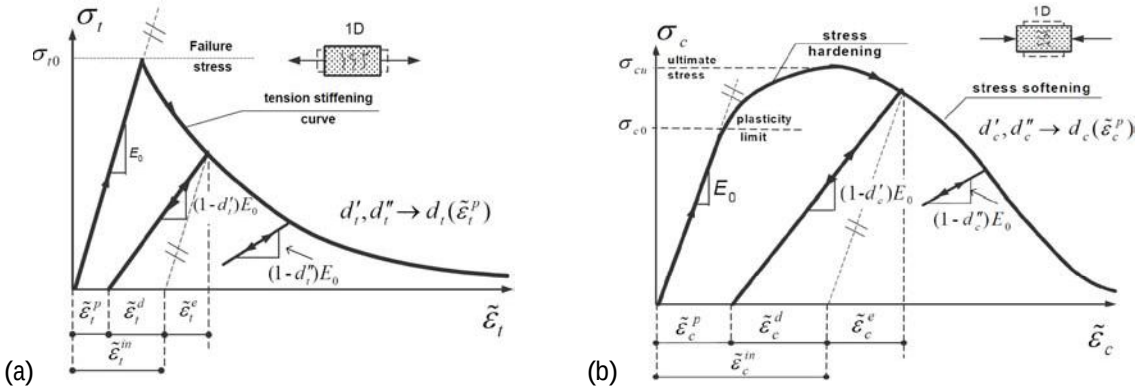

Figure 3. Concrete damage plasticity model in Abaqus/Explicit, response under (a) tension and (b) compression (modified from Wawrzynek and Cincio 2005).

The essential elements of any constitutive model based on the classical plasticity theory are the yield criterion, which determines whether the material shows elastic response at a particular state of stress; the flow rule, which defines the inelastic deformation that occurs when the material yields; and the hardening rule, which defines the way in which the inelastic deformations evolve (Koiter 1960). The yield surface used by Lubliner *et al.* (1989) is an extension of the classical Drucker-Prager model with non-circular deviatoric cross section. The yield surface for the plasticity-based model is represented in Figure 4 and its evolution depends on two hardening variables, $\tilde{\varepsilon}_t^p$ and $\tilde{\varepsilon}_c^p$, in compression and in tension, respectively. It uses a non-associated flow rule and for this reason is suitable for modelling masonry since the joints have extremely low dilatancy (Lourenço 1996). Damage in the plasticity-based model is represented by damage factors, d_t and d_c, that reduce the modulus of elasticity in tension and compression under load reversals by applying the ratios (1-d_t) and (1-d_c), respectively (see Figure 3). When the material unloads and reloads from tension to compression (or vice versa), the compressive and tensile stiffness can be partially recovered. The stiffness recovery in compression and tension is controlled by parameters w_c and w_t, respectively.

The yield surface is defined through the parameters showed in Figure 4. Note that α is a dimensionless coefficient which depends on the compressive yield stresses; f_{c0} is the initial uniaxial compressive yield stress; f_{b0} is the initial biaxial compressive yield stress; f_{t0} is the uniaxial tensile stress at failure; $\overline{p}$ and $\overline{q}$ are the two invariant stresses known as hydrostatic pressure stress and Mises equivalent effective stress, respectively; $\hat{\overline{\sigma}}_1$ and $\hat{\overline{\sigma}}_2$ are the principal effective stresses; and β is a dimensionless coefficient which relates the effective compressive cohesion stress and the effective tensile cohesion stress.

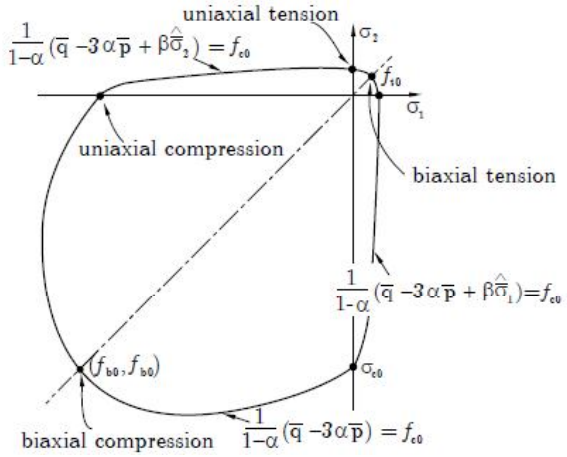

Figure 4. Yield surface for the state of plane stress (modified from Abaqus 6.9 SIMULIA 2009).

In this paper, an exponential and a parabolic curve were selected for modelling the tensile and the compressive behaviour of adobe material in the inelastic range, respectively (see Figure 3). The expressions for representing the hardening and softening curves were defined by Lourenço (1996), and they can take into account the reduced strength of adobe masonry.

SHAKING TABLE EXPERIMENTAL STUDY OF A FULL-SCALE ADOBE BUILDING MODEL

Blondet *et al.* (2006) carried out a dynamic shaking table test on a full-scale adobe model at the Pontificia Universidad Católica del Perú (PUCP) to study the seismic response and damage pattern of a typical Peruvian adobe dwelling. The unidirectional dynamic test was performed on an adobe model built over a reinforced concrete ring beam that anchors the specimen to the unidirectional shaking table. The total weight (including foundation) was around 135 kN. The weight of the concrete beam was 30 kN. The adobe bricks and the mud mortar used for the specimen construction had a soil:coarse sand:straw volume proportion of 5:1:1 and 3:1:1, respectively. The soil was composed of inorganic clay and silt, which is typically used for agriculture. The particle size of coarse sand ranges from 0.5 to 1 mm. The straw for adobe units and mortar consisted mainly of dry grass. The specimen was composed of four walls identified as North (N), South (S), East (E) and West (W) (Figure 5). The displacement signal was applied parallel to the S and N walls. The S and N wall heights were variable, starting at 1.98 m at the intersection with wall E and ending at 2.25 m at the intersection with wall W.

The longitudinal (S and N) walls included a central window opening and the wall E included a door opening. The wall thickness was 250 mm, except for wall N which was 280

mm thick since it was finished with mud plaster on both sides. The mud plaster had a soil:coarse sand:straw proportion identical to that of the mortar. The roof was made of wood joists covered with cement tiles and the joists were connected to the walls with steel nails. The test specimen intended to represent a room in a typical vernacular Peruvian adobe building. The plan dimensions were chosen to suit the limitations of the 4.0x4.0 m shaking table, which allows a 160 kN maximum specimen weight.

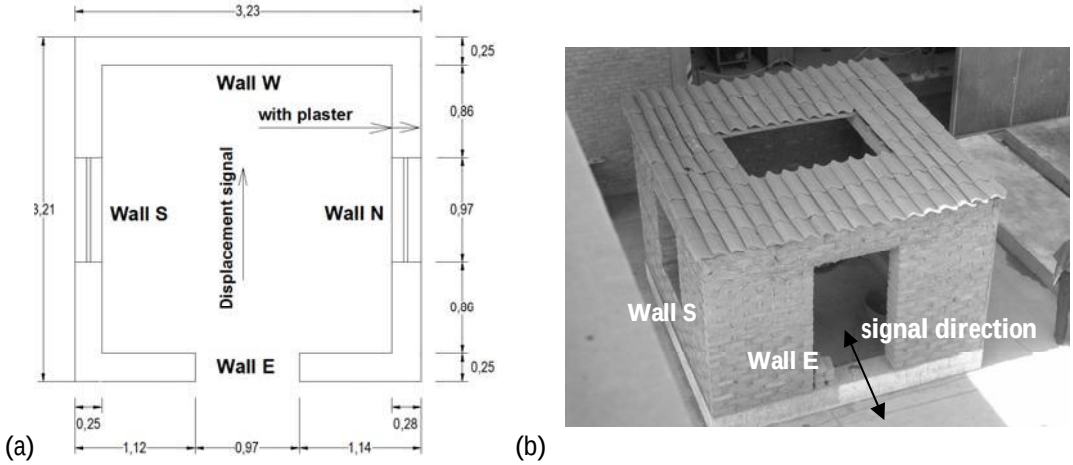

Figure 5. Adobe model tested on the PUCP shaking table, (a) plan dimensions, and (b) a 3-D view.

The specimen was subjected to three levels of unidirectional base-displacement signals, labelled Phase 1, Phase 2, and Phase 3, with maximum displacement amplitudes of 30, 80 and 120 mm, respectively. The displacement input was obtained by processing the acceleration time history record of the May 31st, 1970 earthquake recorded in Lima by the Peruvian Geophysics Institute (Figure 6). This earthquake was characterized by magnitude (Mw) of 7.9 and its epicentre was 375 km away from Lima. The only available record PRQ-7005311523 (available from http://www.cismid-uni.org/redacis/index.php) was scaled to the above-mentioned maximum displacement amplitudes, which correspond to PGA values of 0.3, 0.8, and 1.2 g, respectively. These three earthquake levels represented a frequent, moderate, and severe earthquake relevant for adobe buildings in Peru (Blondet *et al.* 2006; Ottazzi *et al.* 1989). The displacement history applied in Phase 2 of the testing is shown in Figure 7.

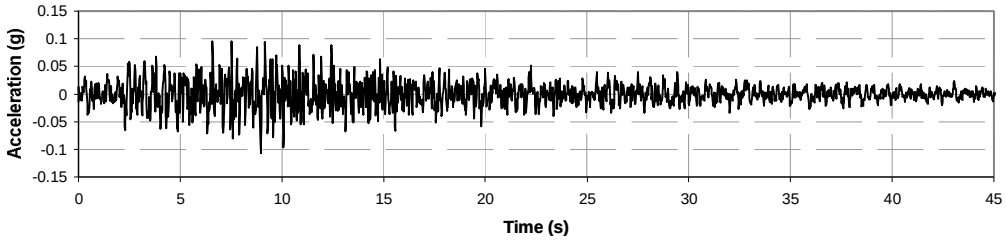

Figure 6. Horizontal EW acceleration record of the May 31st, 1970 earthquake recorded in Lima, Peru.

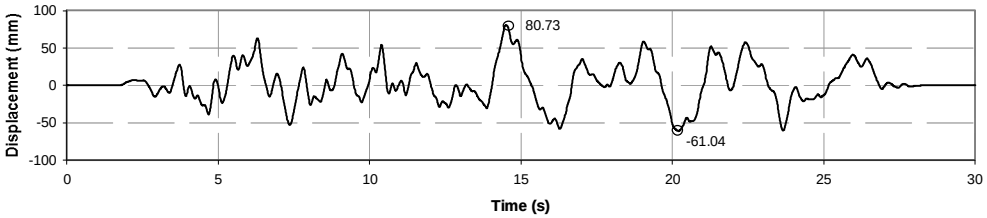

Figure 7. Shaking table displacement input used in Phase 2 (80 mm maximum displacement).

Ten accelerometers and eight LVDTs were used for measuring the accelerations and the displacements in the adobe structure, while an accelerometer and a LVDT were used to control the accelerations and the displacements of the shaking table (Figure 8). The LVDT D7 measured the relative elongation between perpendicular walls N and W.

The model was tested approximately two weeks after the construction. Note that the authors suggest that adobe structures should be tested 30 days after construction, when the tensile strength reaches its maximum value (Vargas *et al.* 1983).

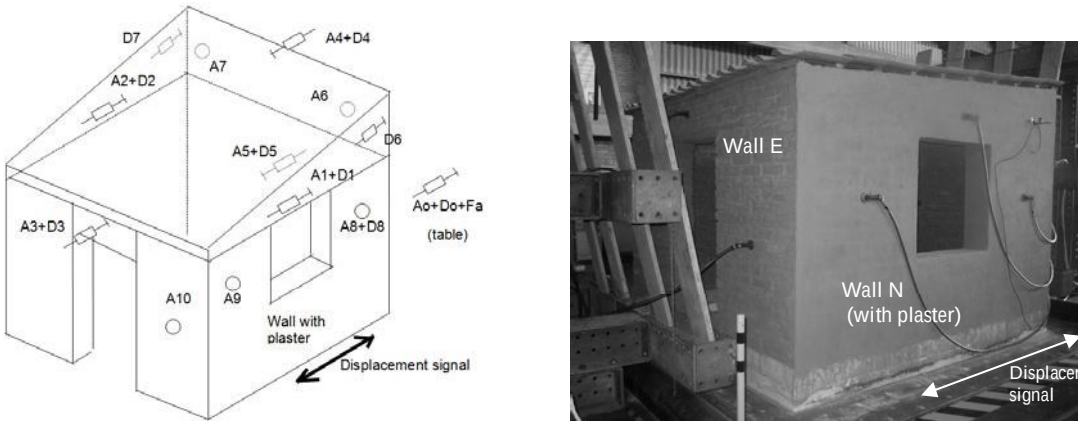

Figure 8. Locations of the accelerometers and LVDTs on the test specimen.

DAMAGE DESCRIPTION

The displacement signals were applied parallel to the S and N walls. At the end of Phase 1 (30 mm maximum displacement input) and during Phase 2 (80 mm maximum displacement input), typical vertical cracks appeared at the wall intersections indicating separation of

transverse walls (E and W) from longitudinal walls (N and S). At the highest displacement levels in Phase 2, X-shaped cracks characteristic of in-plane seismic effects appeared in the longitudinal walls N and S, and flexural cracks appeared in transverse walls E and W due to out-of-plane seismic effects.

As expected, the roof-wall connection in form of steel nail anchorage between the wood joists and adobe walls failed during Phase 2. After the anchorage failure, the roof did not collapse immediately due to friction between the roof system and the walls N and S. Major damage was observed during Phase 2 and a partial collapse occurred during Phase 3 (130 mm maximum displacement input).

During Phase 2, wall W disintegrated into three rigid blocks, typical of walls supported at the base and at the two vertical sides, showed out-of-plane rocking behaviour. During Phase 3, walls E and W overturned at the beginning of the signal input while walls S and N were completely cracked. However, the roof did not collapse because it was supported by walls N and S, which were severely damaged but did not collapse.

Size of vertical cracks at the wall intersections increased with the signal amplitude. From the displacement histories reported by the LVDTs during Phase 2, it was seen that all walls had a maximum relative displacement right after 10 s, when the vertical cracks reached their maximum size. Thereafter, the two longitudinal walls (walls N and S) moved as a rigid body, while the two perpendicular walls (E and W) moved back and forth showing rocking behaviour. The formation of vertical cracks caused wall separation, allowing them to move independently of one another. Figure 9 shows the damage in the adobe model at the three different phases. Plastered wall N was stiffer than wall S due to its larger thickness. The difference in stiffness between walls N and S triggered torsional effects in the structure during Phases 2 and 3. The remainder of this paper discusses the results of numerical simulations of the above described shaking table tests, with the focus on Phase 2 experimental results.

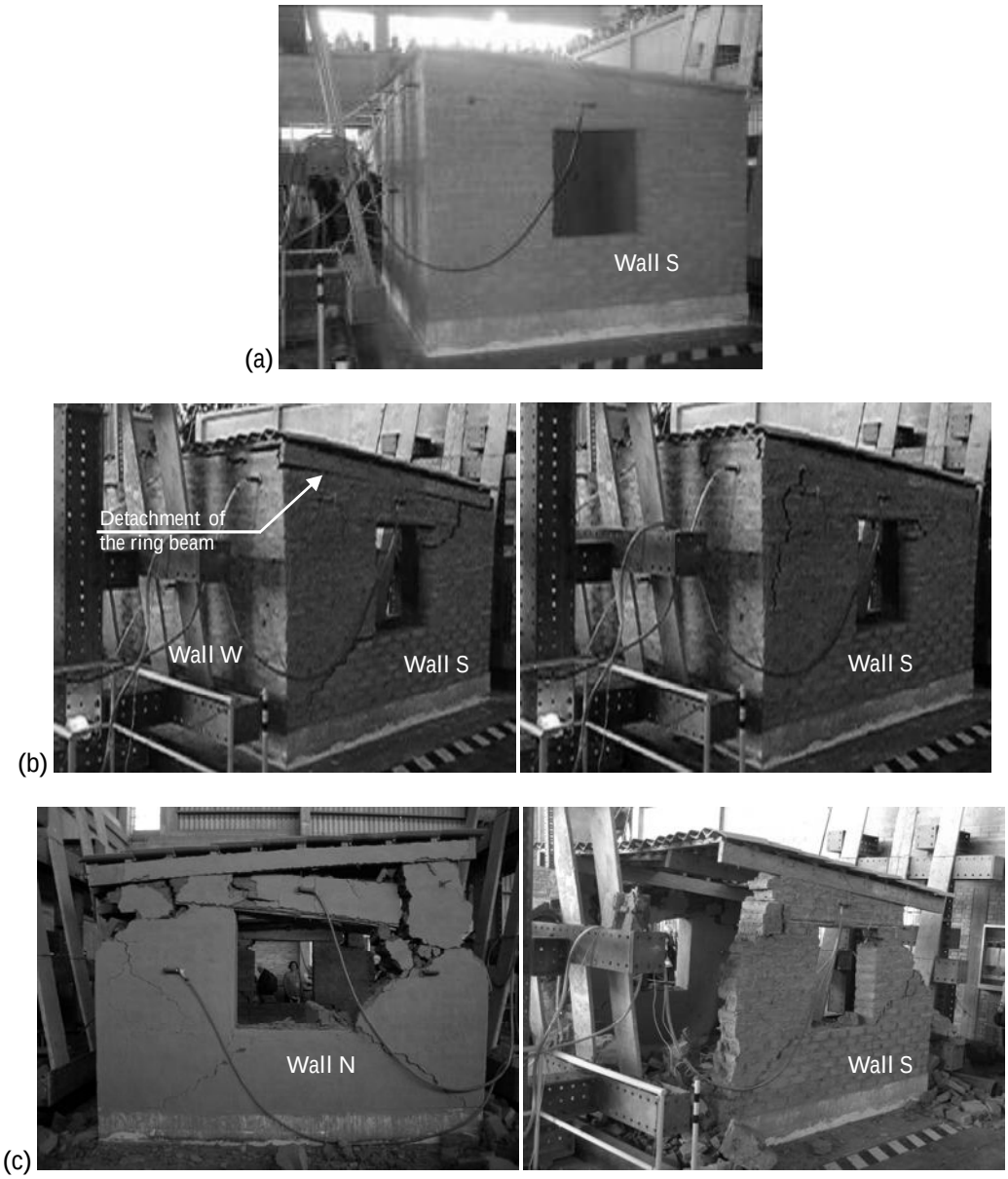

Figure 9. Adobe building model during and after the shaking table tests, (a) the model at the end of Phase 1, showing small cracks that appeared at the wall intersections; (b) the model during Phase 2, showing visible diagonal and vertical cracks, and (c) the model at the end of Phase 3.

NUMERICAL STUDIES

CALIBRATION OF THE MATERIAL PROPERTIES

In a previous work by Tarque (2011) the material properties of adobe were calibrated to be used in numerical models. The elastic properties were obtained from previous experimental studies performed at PUCP (Blondet and Vargas 1978): modulus of elasticity (200 MPa), Poisson's module (from 0.15 to 0.25), compression strength of adobe cubes (from 1.20 to 1.80 MPa, mean value 1.44 MPa), compression strength of adobe prisms (from 0.74

to 0.96 MPa, mean value 0.83 MPa), and tensile strength from diagonal compression tests (from 0.013 to 0.033 MPa, mean value 0.026 MPa). The soil used for adobe units and mud mortar was obtained from a farm field in Lima (Peru). In order to define non-linear properties of the material constitutive laws, Tarque (2011) developed a finite element model (shown in Figure 2) to analyze the results of a cyclic testing of an adobe wall carried out at the PUCP (Figure 10). A parametric study was performed by varying the unknown material properties (*e.g.* tension, compression, and shear) to match the numerical results with the experimental force-displacement curve and the failure crack pattern considering a monotonic (Figure 11) and cyclic behaviour (Figure 12).

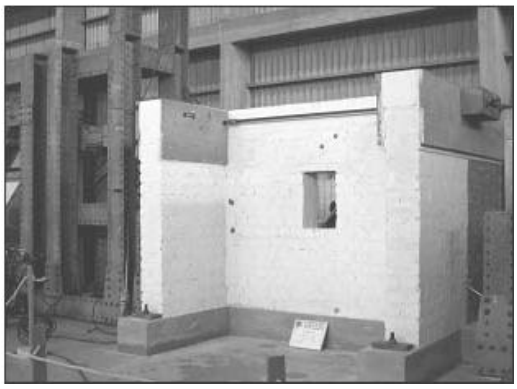

Figure 10. Adobe wall specimen subjected to cyclic lateral loading (Blondet *et al.* 2005).

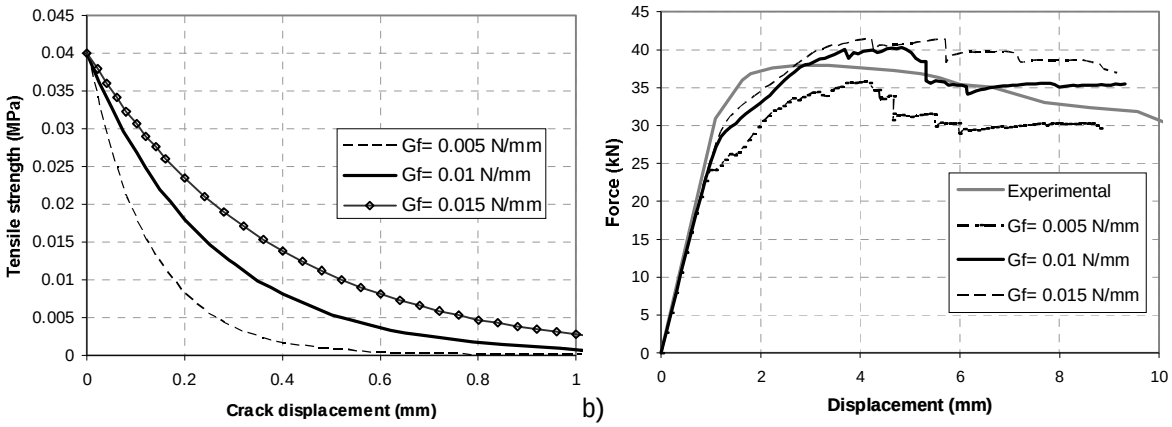

Figure 11. Example of (a) variation of the inelastic part of the tension constitutive law and its influence on the (b) envelope of the force-displacement curve (Tarque 2011).

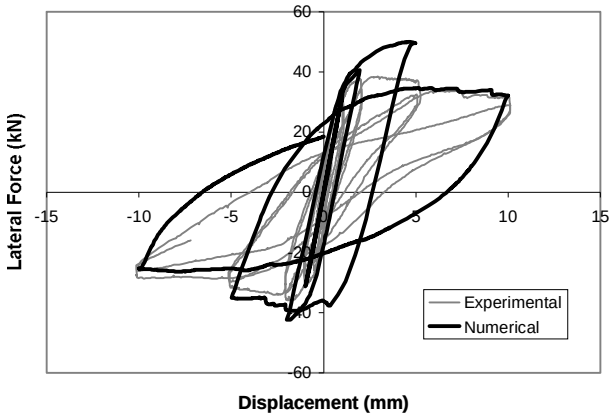

Figure 12. Comparison of experimental and numerical force-displacement curves using the calibrated material properties (Tarque 2011).

MODEL AND MATERIAL PROPERTIES DESCRIPTION

A finite element model was created using Abaqus/Explicit software to simulate Phase 2 experimental response using non-linear dynamic analysis (Figure 13). The foundation (concrete ring beam), the adobe walls, the lintels and two internal wooden beams were represented by shell elements with 6 degrees of freedom (DOF) per node. The other wooden beams (placed above the walls with windows) and the wooden joists were modelled using beam elements. The foundation was fully fixed at the base during the application of gravity loads. After static application of the vertical load, a displacement DOF in the direction of the movement was released at the base nodes to apply the acceleration signal.

The model had 3406 nodes, and it consisted of 232 linear line elements (B31 type in Abaqus), 3038 quadrilateral 4-node shell elements (2x2 integration points, S4 type in Abaqus), and 6 triangular 3-node shell elements (3 integration points, S3 type in Abaqus). All wall elements had 5 Gauss integration points through the thickness to account for out-of-plane bending. The thickness of wall N was 280 mm due to the presence of mud plaster on both sides, while other walls had thickness of 250 mm. The mesh size was kept as close as possible to 100 x 100 mm, thus characteristic length *h* was equal to 141.4 mm. The total mass of the model was 14.21 N.s^2/mm, including the concrete foundation and all wooden elements.

Wooden beams at the roof perimeter were poorly connected at the corners, thus allowing vertical cracks to develop at the wall corners during the test. In other words, the perimeter wooden beams did not exert a continuous top ring beam action on the walls. Consequently, in the numerical model, the wooden beams were not connected to one another at the corners (Figure 13). The internal wooden beams were modelled using shell elements to simulate

evenly distributed stresses and avoid stress concentrations at the contact points between wooden beams and adobe walls.

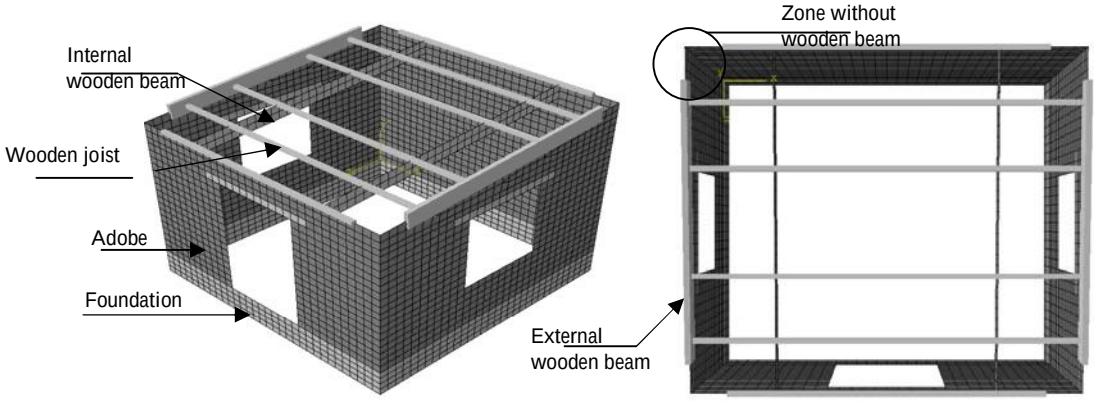

Figure 13. Finite element model of the adobe building model.

Concrete foundations and wooden beams were modelled as elastic elements, whereas the adobe walls were modelled using the concrete damage plasticity model presented earlier in this paper. Elastic material properties for adobe were obtained from previous experimental studies and subsequently calibrated by Tarque (2011). The results are summarized in Table 1 and

Table 2 and Figure 14. When adobe is subjected to load reversals, as in the case of dynamic analysis, it is necessary to numerically represent the process of crack opening and closing by selecting appropriate damage factors and stiffness recovery (see unloading branch in the constitutive laws in Figure 3). These parameters were calibrated numerically by Tarque (2011) using experimental data obtained from cyclic tests on adobe wall specimen discussed earlier in this paper. The damage factors affect the modulus of elasticity when a certain tensile plastic displacement value has been reached, as shown in Figure 3. The following pairs of tensile damage factors (d_t) and tensile plastic displacements were specified: (0.00; 0.00), (0.85; 0.125), (0.90; 0.25), (0.95; 0.50). The stiffness recovery was set to 0.5 in compression (w_c) and 0.0 in tension (w_t). The characteristic length (h) for the elements was 141 mm. The tensile plastic displacement is equal to the plastic strain times the characteristic length.

Table 1. Elastic material properties for concrete and timber (Tarque 2011).

Concrete			Timber		
E (MPa)	υ	γ_m (N/mm^3)	E (MPa)	υ	γ_m (N/mm^3)
22000	0.25	2.4e-05	10000	0.15	6.87e-06

Table 2. Material properties for the adobe masonry modelled using the concrete damage plasticity model in Abaqus (Tarque 2011).

Elastic				Tension		Compression		
E (N/mm^2)	υ	γ_m (N/mm^3)	h (mm)	f_t (N/mm^2)	G_f^I (N/mm)	f_c (N/mm^2)	G_f^c (N/mm)	ε_p (mm/mm)
200	0.2	2e-05	141.4	0.04	0.01	0.45	0.155	0.002

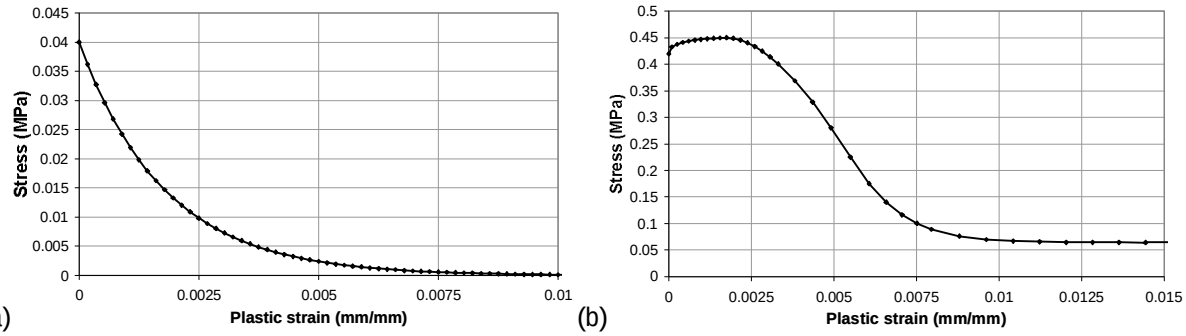

Figure 14. Constitutive stress-strain law for the adobe material, (a) uniaxial tensile, and (b) uniaxial compressive.

The definition of the yield surface for the concrete damage plasticity model requires four additional parameters: the dilation angle, the eccentricity, the ratio of the initial equibiaxial compressive yield stress to initial uniaxial compressive yield stress, and a parameter that defines the shape of the yield surface in the deviatoric plane, k_c.

The angle of dilation controls an amount of plastic volumetric strain developed during plastic shearing. Clays are characterized by a very low amount of dilation. According to Lourenço (1996), the masonry joints have extremely low dilatancy. In this paper the dilation angle was defined as low as possible, thus a value of 1° was used for the analyses. The flow potential eccentricity is assumed to be 0.1, which implies that the material has almost the same dilation angle over a wide range of confining pressure stress values. The ratio between initial equibiaxial and uniaxial compressive yield stress is specified as 1.16 because the material is subjected to equal compression stresses (Park and Paulay 1979). Note that k_c is assumed to be equal to 2/3rd typical value for damage plasticity model.

NUMERICAL ANALYSES AND RESULTS

In the first step of the analysis, gravity loads were applied using an implicit strategy in Abaqus/Standard software. The model was subsequently uploaded into Abaqus/Explicit and the horizontal acceleration in Phase 2 of the testing was applied at the base of the structure. It

was decided to carry out the dynamic analyses within an explicit procedure in order to avoid problems due to large distortions and localized strains. Abaqus/Explicit software makes use of the central difference integration rule for integration of the equations of motion, which is more suitable when dealing with dynamic problems. The global stable time increment computed by Abaqus/Explicit was 4.5018×10^{-06} s. The analyses were performed considering double-precision computations which were recommended to obtain accurate results when a large number of time steps is required. It was assumed that the energy dissipation in the model occurs solely due to the hysteretic behaviour of adobe material, thus no additional damping was imposed.

The cracking pattern observed in the numerical results simulated fairly well the pattern observed in the experimental test. At around 3 s after the application of the base acceleration, vertical cracks appeared at the wall corners (mainly at the contact between walls W and S) and at the ends of door lintels. After approximately 7 s, cracks due to out-of-plane bending appeared in walls E and W which were perpendicular to the direction of applied motion. Diagonal cracks appeared first in wall S at 9 s and then in wall N at 11 s. Cracks at the wall intersections triggered the out-of-plane rocking behaviour of walls E and W. The damage patterns observed in the analyses of walls N and S match the damage observed in the experimental test. Because of the additional thickness of wall N, this wall experienced less damage than wall S. Also, some crushing took place at the base of walls E and W due to out-of-plane rocking. Snapshots of the damage pattern obtained from the analyses are reported in Figure 15 at 10, 20 and 30 s of the acceleration signal.

The absence of an effective top ring beam led to early detachment between orthogonal walls. The numerical results showed that vertical cracks formed at the wall intersections and triggered out-of-plane rocking of the transverse walls perpendicular to the applied base motion; this damage pattern was in compliance with the dynamic experimental test results. Two additional models were developed to evaluate the influence of wooden beams on the dynamic response and crack pattern in the walls. The first model was created considering a complete, continuous ring beam above the walls, while the second model did not include the wooden beams. Neither model was able to match the experimental results. In the first model, the vertical cracks at the wall intersections and the out-of-plane deformations of walls E and W were restricted due to the ring beam confinement effects at the wall corners (Figure 16a). In the second model, wall W showed large displacements and overturning and did not capture

correctly the experimental out-of-plane rocking (Figure 16b). Thus, the best assumption was to consider the wooden beams disconnected at the corners, as seen in Figure 13.

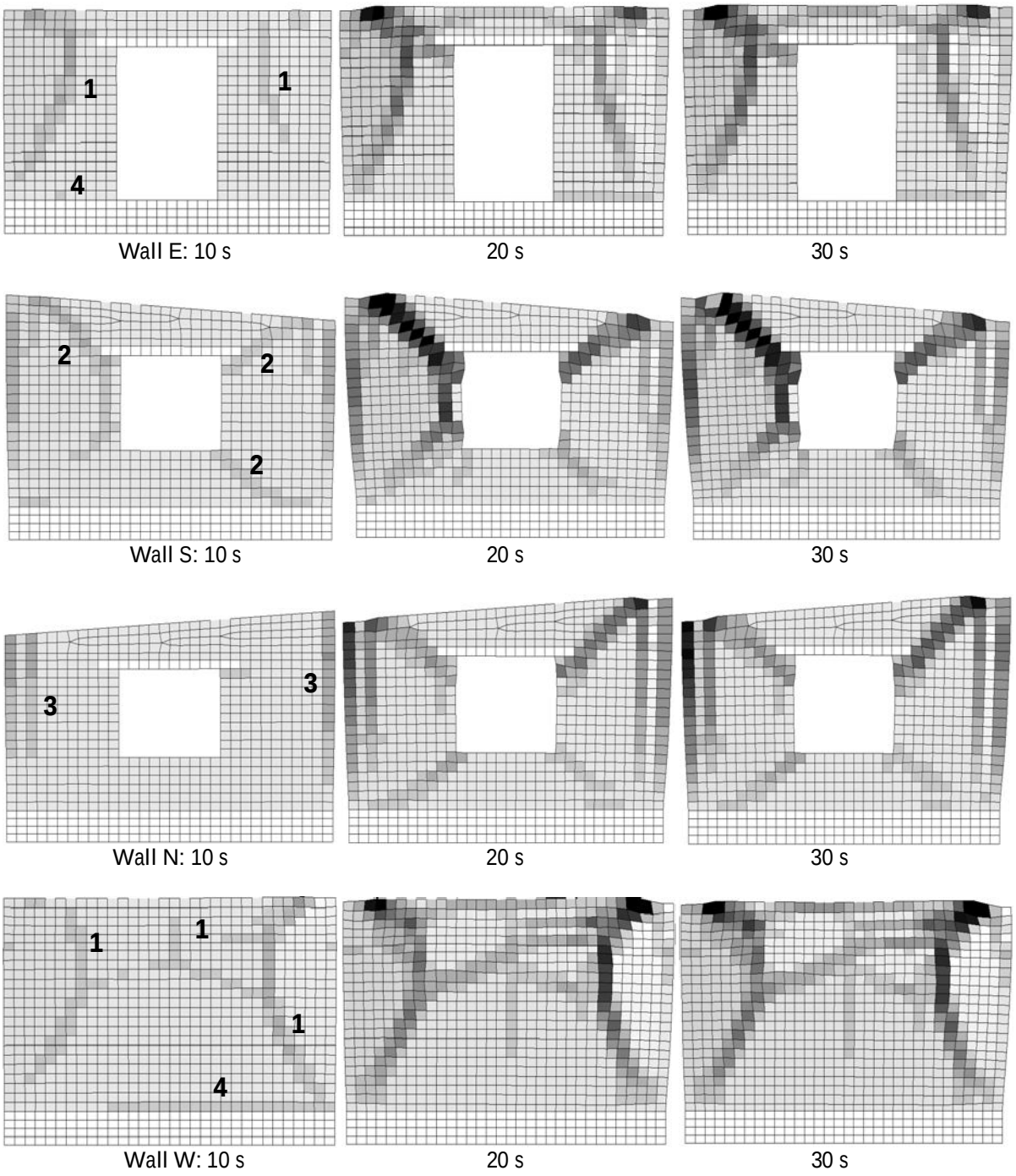

Maximum tensile plastic strain values						
0 to 9.92E-02	9.92E-02 to 1.74E-01	1.74E-01 to 2.48E-01	2.48E-01 ; 3.98E-01	3.98E-01 to 5.47E-01	5.47E-01 to 6.96E-01	6.96E-01 to 8.45E-01

Figure 15. Progression of the tensile plastic strain of the numerical model at 10 s, 20 s and 30 s: (1) cracking due to bending, (2) cracking due to in-plane seismic effects, (3) vertical cracking, and (4) crushing (deformation scale= 1).

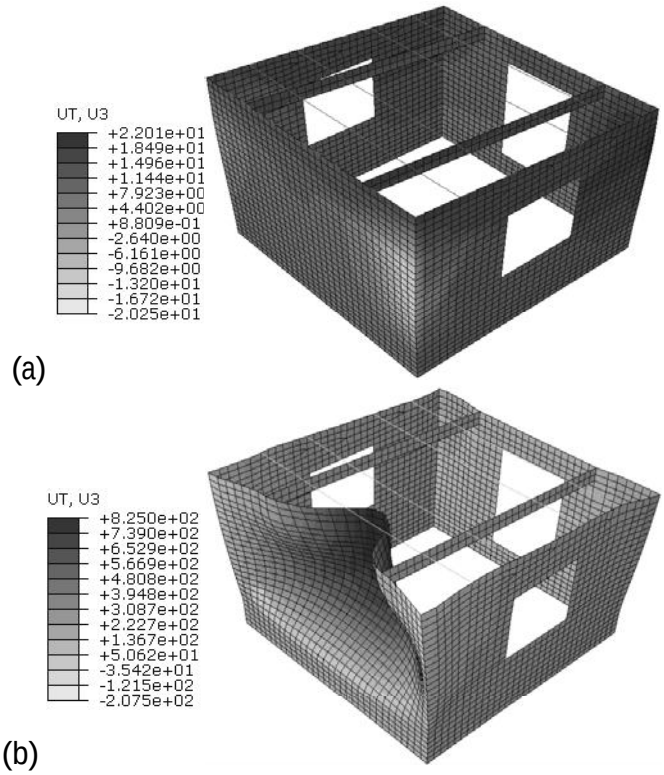

Figure 16. Deformation at the end of the input signal (30 *s*): (a) model with complete ring beam, and (b) model without ring beams (deformation scale= 1).

Figure 17 shows the damage factor plot for the model. The light coloured areas represent the regions where the model experienced less damage. The damage was concentrated at the wall intersections and transverse walls perpendicular to the base motion (E and W); this is similar to the experimental findings. High bending stresses caused localized damage at wall intersections.

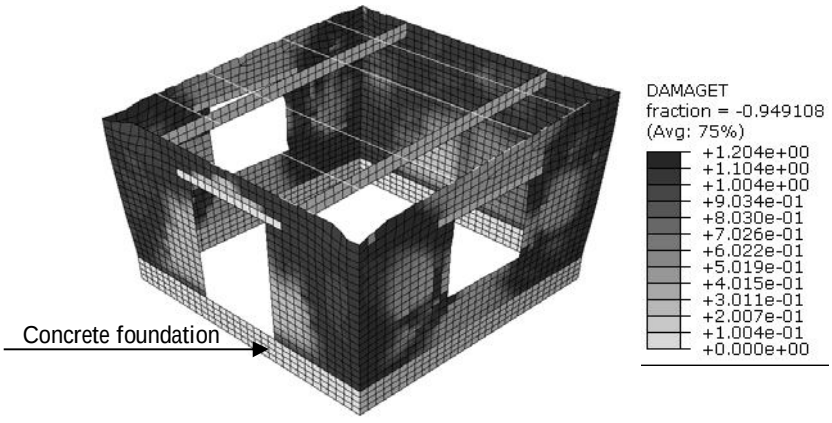

Figure 17. Tensile damage factor for the numerical model.

Figure 18 compares the experimental and numerical displacement time histories. In both cases the maximum relative displacement occurred at around 10 s. Afterwards, the walls oscillated around a new equilibrium position indicating a residual inelastic displacement. The

numerical rocking behaviour of transverse walls E and W (out-of-plane) differed in amplitude from the experimental behaviour; since the numerical model was continuous, it was not possible to simulate physical separation of the walls (Figure 9c), and a subsequent independent vibration of the perpendicular walls. In the experimental test, the walls started to move independently once the corners were fully cracked, whereas in the numerical analysis the displacements of walls E and O were not completely independent from walls N and S due to limitation of the numerical model. This limitation could be potentially solved by providing interface elements between the wall corners, however the interface properties would be very difficult or impossible to calibrate. In spite of its limitations, the numerical model captured the main structural properties and global behaviour, namely the wall natural frequency, the damage evolution, and failure pattern.

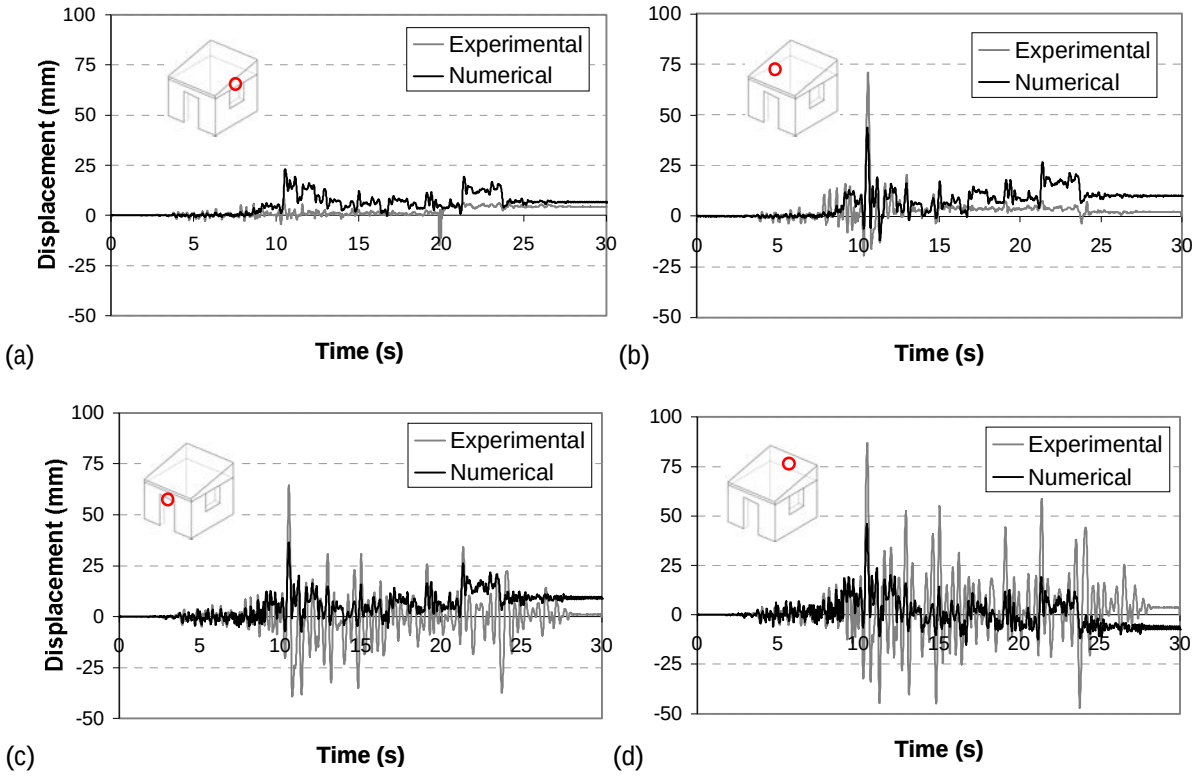

Figure 18. Experimental and numerical displacement histories of the adobe walls measured at the top center of the (a) wall N, (b) wall S, (c) wall E, and (d) wall W.

ENERGY BALANCE

When dealing with an explicit method of analysis, one way to check numerical convergence is to control the energy balance of the whole system. The energy balance of the

model should be constant and close to zero during all the analysis. The energy balance of the entire model is given by:

$$E_{total} = E_{KE} + E_I + E_{VD} - E_W \quad (1)$$

where E_{KE} is the kinetic energy, E_I is the total internal energy, E_{VD} is the visco-elastic energy and E_W is the work done by the external actions. In the dynamic model of the adobe model the total internal energy is given by:

$$E_I = E_{SE} + E_{PD} + E_{DMD} + E_{AE} \quad (2)$$

where E_{SE} is the recoverable strain energy, E_{PD} is the energy due to plastic dissipation, E_{DMD} is the energy dissipated by damage, and E_{AE} is the artificial energy.

Figure 19a shows the energy components. It is seen that the greater contribution of the plastic energy is clear, which is an indication of the progressive model damage. As specified in Behbahanifard *et al.* (2004) and Harewood and McHugh (2007), the E_{AE} should be less than 5% of the physical internal energy given by E_{SE}+E_{PD}+E_{DMD}. Figure 19b shows that the energy balance from equation (1) was almost zero throughout the analysis; this indicates that the explicit analysis does not diverge.

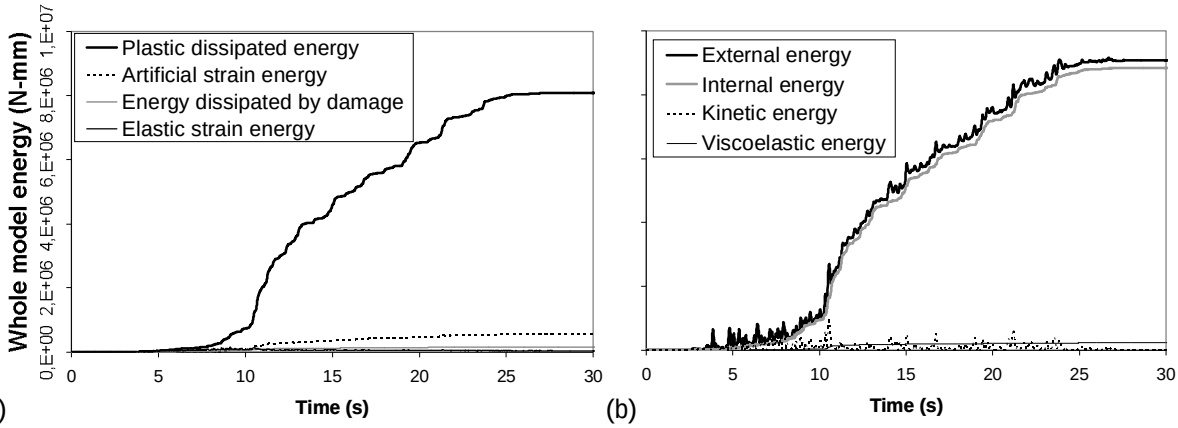

Figure 19. Variation of the numerical model energy balance: (a) components of the total internal energy, (b) energy components for the energy balance.

CONCLUSIONS

This paper deals with the non-linear dynamic analysis of an adobe model, previously tested at the Pontificia Universidad Católica del Perú, following a continuum approach in Abaqus/Implicit and Abaqus/Explicit finite element software package. To model the adobe masonry, the concrete damage plasticity constitutive model implemented in Abaqus was

used. Adobe masonry was treated as a homogeneous material and it was represented by its tensile and compressive constitutive laws. The material properties (elastic and inelastic) were calibrated in a previous study by Tarque (2011), based on the results of an experimental study on in-plane cyclic response of an adobe wall. A need for additional experimental research to quantify the material parameters of adobe masonry in mud mortar was recognized.

The numerical model was subjected to an acceleration record at the base to simulate experimental model during the Phase 2 of the experimental study, which produced the maximum base displacement of 80 mm. The numerical results represented fairly well the response frequencies, the crack pattern, the failure mechanisms and displacement response observed in the test. Poor connection between the wooden beams at the roof perimeter and the adobe walls observed in the experimental study was simulated by disconnecting the wooden beam elements at the wall corners (see Figure 13); this allowed for separation of orthogonal walls at the wall intersections, as observed in the experimental study.

The calibrated material properties proposed by the authors and the analysis model proved to be useful for studying the non-linear dynamic response of adobe buildings under seismic excitations. It was shown that a commercial finite element software package can be used to perform advanced non-linear analyses for the purpose of seismic vulnerability assessment of highly brittle existing adobe buildings. The approach taken in this study can be extended to other adobe building typologies in order to predict the seismic behaviour of different structural configurations and evaluate possible strengthening solutions. A key issue associated with modelling seismic behaviour of real adobe structures is the correct representation of the roof system and its connections, and it should be carefully addressed.

Previous numerical studies by the authors encountered severe convergence problems when dealing with brittle materials combined with implicit solution strategies. The explicit procedure followed in this study proved reliable and allowed simulation of the test results during the entire 30 s earthquake time history record without experiencing divergence problems; this showed that explicit strategies are viable for non-linear finite element analyses of brittle structures such as adobe and unreinforced masonry buildings.

REFERENCES

Abaqus 6.9 SIMULIA, 2009. *Abaqus/CAE Extended Funcionality EF2*, *Manual*, Dassault Systemss Corporation, Providence, RI, USA.

Behbahanifard, M. R., Grondin, G. Y., and Elwi, A. E., 2004. Analysis of steel plate shear walls using explicti finite element method, *13th World Conference on Earthquake Engineering*, Vancouver, Canada.

Blondet, M., and Vargas, J., 1978. Investigación sobre vivienda rural, *Report*, Division of Civil Engineering, Pontificia Universidad Católica del Perú, Lima, Peru.

Blondet, M., Madueño, I., Torrealva, D., Villa-García, G., and Ginocchio, F., 2005. Using industrial materials for the construction of safe adobe houses in seismic areas, *Proceedings of Earth Build 2005 Conference*, Sydney, Australia.

Blondet, M., Vargas, J., Velásquez, J., and Tarque, N., 2006. Experimental Study of Synthetic Mesh Reinforcement of Historical Adobe Buildings, *Structural Analysis of Historical Constructions*, P. B. Lourenço, P. Roca, C. Modena, and Agrawal. S., eds., New Delhi, India, pp. 1-8.

Cruz, J. S., Barros, J., and Azevedo, Á., 2004. *Elasto-plastic multi-fixed smeared crack model for concrete*, *Report* 04-DEC/E-05, University of Minho, Minho, Portugal.

Feenstra, P. H., and de Borst, R., 1992. The use of various crack models in F.E. analysis of reinforced concrete panels, *First International Conference on Fracture Mechanics of Concrete Structures: FraMCoS1*, Z. P. Bažant, ed., Colorado, USA.

Feenstra, P. H., and Rots, J. G., 2001. Comparison of Concrete Models for Cyclic Loading, *Modelling of Inelastic Behaviour of RC Structures under Seismis Loads*, P. B. Shing and T.-aki Tanabe, eds., American Society of Civil Engineers, USA, pp. 38-55.

Harewood, F. J., and McHugh, P. E., 2007. Comparison of the implicit and explicit finite element methods using crystal plasticity, *Computational Materials Science*, Vol. 39, No.2, pp. 481-494.

National Institute of Statistics and Informatics (INEI), 2008. *Census 2007: XI de Población y VI de Vivienda*, Peru, http://iinei.inei.gob.pe/iinei/RedatamCpv2007.asp?id=ResultadosCensales?ori=C, accessed on 14th november 2011.

Koiter, W. T., 1960. General theorems for elastic-plastic solids, *Progress in Solid Mechanics*, I. N. Sneddon and R. Hill, eds., North Holland Publishing Company, pp. 165-221.

Lee, J., and Fenves, G. L., 1998. Plastic-Damage Model for Cyclic Loading of Concrete Structures, *Journal of Engineering Mechanics*, Vol. 124, No.8, pp. 892-900.

Lotfi, H. R., and Shing, P. B., 1994. Interface Model Applied to fracture of masonry Structures," *ASCE*, Vol. 120, No.1, pp. 63-80.

Lourenço, P. B., 1996. Computational strategies for masonry structures, *Ph.D. Thesis*, Delft University, Delft, The Netherlands.

Lubliner, J., Oliver, J., Oller, S., and Oñate, E., 1989. A plastic-damage model for concrete, *International Journal of Solids and Structures*, Vol. 25, No.3, pp. 299-326.

Memari, A. M., and Kauffman, A., 2005. Review of Existing Seismic Retrofit Methodologies for Adobe Dwellings and Introduction of a New Concept, *SismoAdobe2005*, Pontificia Universidad Católica del Perú, Lima, Peru, p. 15.

Ngo, D., and Scordelis, A. C., 1967. Finite Element Analysis of Reinforced Concrete Beams,"*American Concrete Institute*, Vol. 64, No.3, pp. 152-163.

Ottazzi, G., Yep, J., Blondet, M., Villa-García, G., and Ginocchio, F., 1989. *Ensayos de simulación sísmica de viviendas de adobe*, *Report*, Division of Civil Engineering, Pontificia Universidad Católica del Perú, Lima, Peru.

Park, R., and Paulay, T., 1979. *Reinforced Concrete Structures*. LIMUSA Eds, Mexico, 800 pp.

Page, A. W., 1978. Finite element model for masonry, *Journal of Structural Engineering*, Vol. 104, No.8, pp. 1267-1285.

Pelà, L., 2008. Continuum damage model for nonlinear analysis of masonry structures, *Ph.D. Thesis*, Università degli Studi di Ferrara, Ferrara, Italy.

Roca, Pere, Cervera, M., Gariup, G., and Pela, L., 2010. Structural Analysis of Masonry Historical Constructions. Classical and Advanced Approaches, *Archives of Computational Methods in Engineering*, Vol. 17, No.3, pp. 299-325.

Rots, J. G., 1991. Numerical simulation of cracking in structural masonry, *Heron*, Vol. 36, No.2, pp. 49-63.

Tarque, N., Crowley, H., Pinho, R., and Varum, H., 2012. Displacement-Based Fragility Curves for Seismic Assessment of Adobe Buildings in Cusco, Peru, *Earthquake Spectra*, Vol. 28, No.2, pp. 759–794.

Tarque, N., 2011. Numerical modelling of the seismic behaviour of adobe buildings, *Ph.D. Thesis*, ROSE School, Istituto di Studi Superiori di Pavia IUSS, Pavia, Italy.

Vargas, J., Bariola, J., Blondet, M., Mehta, P.K., Villa García, G., and Ginocchio, F., 1983. *Investigación Científica Innovativa: Edificaciones de adobe en áreas sísmicas. Project AID 936/5542*, *Report*, Division of Civil Engineering, Pontificia Universidad Católica del Perú, Lima, Peru.

Wawrzynek, A., and Cincio, A., 2005. Plastic-damage macro-model for non-linear masonry structures subjected to cyclic or dynamic loads, *Conf. Analytical Models and New Concepts in Concrete and Masonry Structures, AMCM'2005*, Gliwice, Poland.